

NPS-58G172071A

NAVAL POSTGRADUATE SCHOOL

Monterey, California



THE DEVELOPMENT OF A HOMOGENEOUS NUMERICAL
OCEAN MODEL FOR THE ARCTIC OCEAN

by

J. A. Galt

July 1972

Approved for public release; distribution unlimited

NAVAL POSTGRADUATE SCHOOL
Monterey, California

Rear Admiral A. S. Goodfellow, USN
Superintendent

Milton U. Clauser

ABSTRACT:

A numerical ocean model driven by surface stress and a source-sink distribution is developed for a homogeneous ocean. Non-linearities, lateral friction and bottom friction are included. The basin shape can be varied to accommodate a large variety of configurations. Variable bathymetry and sources/sinks around the perimeter are included. The numerical scheme is conditionally stable and has second order accuracy in space and time.

A number of test cases are run to explore the dynamic significances of the various processes represented. The possible influence of these processes on the circulation of the Arctic ocean are discussed.

TABLE OF CONTENTS

Section I - Introduction and Report Summary	4
Section II - Development of the First Stage Numerical Model .	8
Section III - Preliminary Results	21
Section IV - Future Model Plans	32
References	34
Appendix - Use of Computer Program	36

LIST OF FIGURES

- Figure 1. Chart of the Arctic Basin with the 100, 1000 and 2000 fathom depth contours drawn. Cross indicates location of the North Pole.
- Figure 2. Grid pattern used in finite difference scheme and numbering system used for calculational molecule.
- Figure 3. Configuration of the model used to check out the relaxation of the stream function.
- Figure 4. Streamlines of source-sink driven flow with zero vorticity in the interior and uniform depth
- Figure 5. Streamlines of source-sink driven flow with uniform negative vorticity in the interior and uniform depth.
- Figure 6. Streamlines of flow driven by uniform stress curl in an irregular shaped ocean with a central ridge. (The ridge runs from top to bottom in the figure.)
- Figure 7. Streamlines of flow driven by a simple source-sink distribution for an irregular shaped ocean with a central ridge. (The ridge runs from the top to the bottom in the figure.)

Section I - Introduction and Report Summary

The general equations that describe the flow of both the atmosphere and the ocean are well known and are available to geophysicists for the investigation of a large variety of circulation problems. For many cases of interest analytic solutions to these general equations are not possible because of significant non-linearities in the equations, or because of irregular geophysical boundary configurations, or both. Although analytic solutions are not generally available it is often possible to obtain useful approximate solutions using numerical techniques. This numerical modeling has become a powerful tool for the investigation of both the ocean and the atmosphere.

Large scale numerical models available for the description of many features of the atmosphere and large portions of the oceans can be divided into roughly two groups. The first group is exploratory in nature and is used to investigate the significance of various physical processes. The prime emphasis is to understand just why a particular system responds as it does and what effects variations in forcing have on the outcome. The results from this type modeling may, or may not, be physically realistic but in all cases should elucidate the characteristics of the flow to be expected, its sensitivity to various inputs and significant correlations that are likely to exist. The second group of numerical models is generally more advanced and is designed for forecasting geophysical fluid flow on a more or less real time basis. The relative stage of refinement and the

large amounts of high quality data required for initial conditions has inhibited the development of these type models for the ocean and essentially all of the forecasting models routinely used deal with the atmosphere.

The object of this research was to begin a numerical exploration on the large scale circulation of the Arctic Ocean.

In the past numerical models of the Arctic Ocean have concentrated their attention on the sea ice that overlies most of the Ocean (Campbell, 1965) and tried to answer questions concerning the drift and climatological permanence of the pack ice (Maykut and Untersteiner, 1971). With the exception of Campbell's use of a simplified ocean model under an ice-layer model no significant effort has been directed towards a numerical study of the actual flow of the Arctic Ocean's waters.

At the onset of this research it must be admitted that very little is actually known about Arctic Ocean dynamics and that difficulties can be anticipated in deciding on appropriate boundary conditions and input parameters for the model. In many cases field data from the Arctic is lacking, or inadequate to give the required stress fields or inflow-outflow conditions with sufficient accuracy. This then demands that best estimates of boundary conditions serve as a tentative guide and that wide ranges of parametric inputs actually be investigated. The resulting numerical exploration yields considerable insight into the relative significance of various oceanographic parameters.

In addition to the uncertainties related to the lack of actual input data the development of a new numerical model has potential difficulties

inherent in the finite difference mathematic's that must be used. Both these problems can best be addressed by the careful development of the model from simple to more complex cases in a stepwise progression and with each step being checked against any available data (from the field or analytic considerations). This model is carried through this sort of genesis.

The first step in the model to be used for the Arctic assumes homogeneous water and variable depth which is in some way similar to a model used by Holland (1976). The grid system used is based on a triangular plan similar to some systems used by Williamson (1968) and Sadourny, Arakawa and Mintz (1967). Both lateral and bottom friction are included in the model. The flow is driven by stress applied at the surface (simulating the wind or ice stress) and by source-sink distributions around the edge (that simulates major channels between the Arctic and other oceans). The details of the development for this first step in the model are given in the next section. The initial check out and experimentation with this first stage in the development of an Arctic Ocean circulation model has led to some interesting results. In particular: 1) negative curl introduced into the flow results in current patterns resembling the Beaufort Gyre; and 2) the Lomonosov Ridge (Fig. 1) acts like a dynamic block which may greatly increase the significance of the circulation caused by the source-sink distribution. There is some indication from field data reported by Muench (1970) and Thorndike (1971) that the processes indicated in the model have some counterpart in actual circulation observed

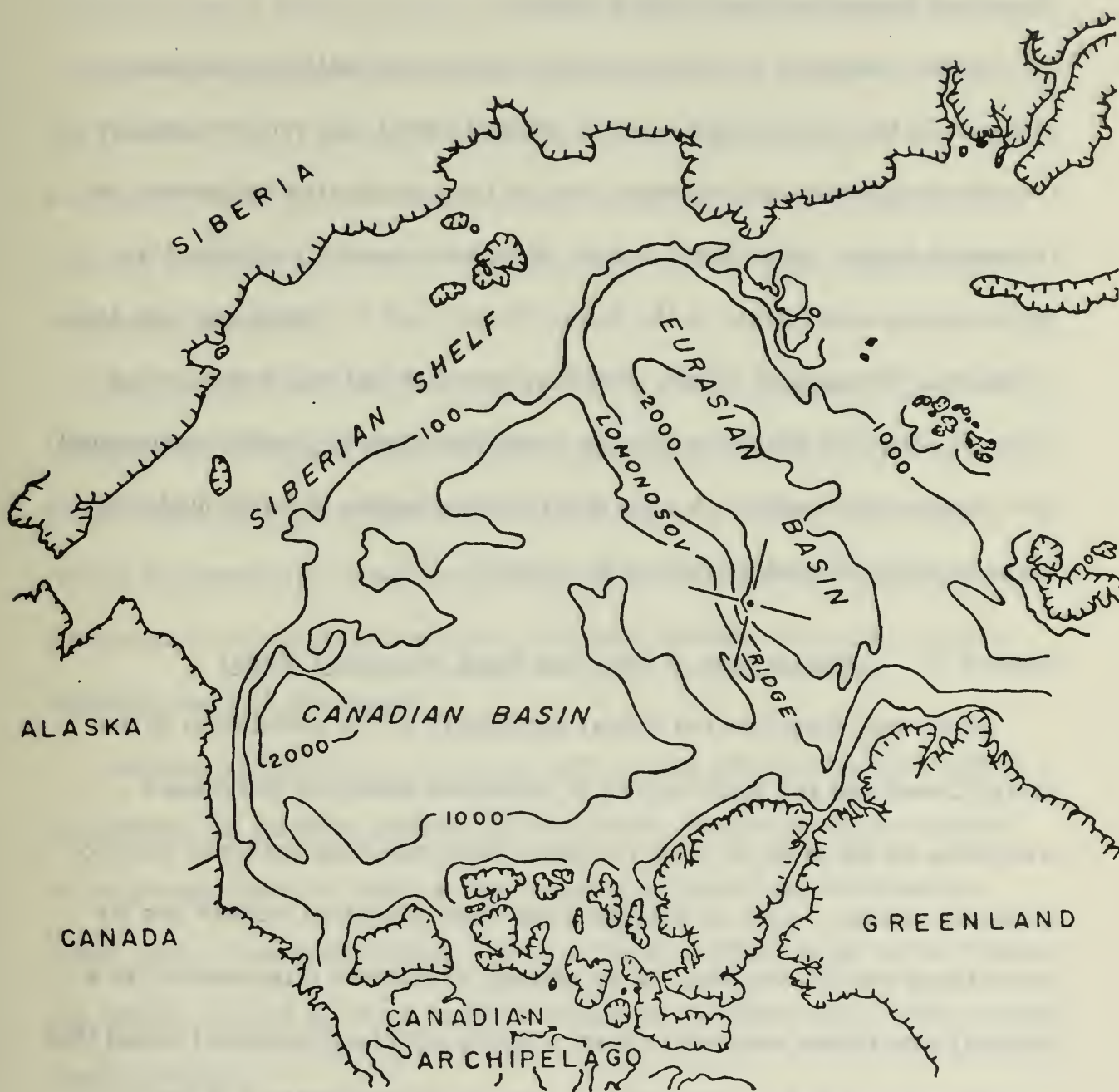


Figure 1. Chart of the Arctic Basin with the 100, 1000 and 2000 fathom depth contours drawn. Cross indicates location of the North Pole.

in the Arctic Ocean. A more detailed discussion of these results are presented in section three of this report.

Future extension and development of the model will be continued in stages. In the immediate future the present model will run with greatly increased resolution to delineate more of the complicated bathymetry of the Arctic Basin. After those results have been carefully explored the stratification appropriate to the Arctic Ocean must be introduced into the modeling. The results for the stratified ocean model will indicate how the next step (the inclusion of more complicate thermodynamic exchanges) can best be approached. A more detailed discussion of future modeling plans is given in section four of this report.

Section II - Development of the First Stage Numerical Model

When one considers the actual complexity of the circulation in the Arctic Ocean and the wide variety of numerical modeling techniques available for its study it is by no means obvious which path will lead to maximum returns. Each of the presently used numerical models has its advantages and limitations. In an attempt to address this question in a rational way it was decided to start with the simplest numerical model that could simulate what are thought to be the dominant forcing and geomorphology in the Arctic.

There can be little doubt that much of the large scale circulation of the Arctic Ocean is wind driven either directly, or indirectly through an ice cover that acts as some sort of coupling element (Campbell, 1965).

The details of how the ice cover couples the atmosphere to the ocean and to what extent it filters the time and space variations are unknown. There is however, a substantial effort directed towards this problem (Untersteiner, and Fletcher, 1971) and some progress can be anticipated. For the present model these interesting questions can not be treated in detail and thus the stress on the top of the ocean will be considered a known field, externally specified.

Studies by Coachman and Barnes (1961, 1963), Aagaard (1966) all indicate that there may be dynamically significant exchange between the Arctic Basins and the adjacent portions of the world ocean. For this reason the numerical model incorporates sources and sinks of water around its perimeter to simulate the major channels between the Arctic and the adjacent parts of the ocean.

Looking at Figure 1., it is seen that a large fraction of the Arctic is covered by the relative shallow Siberian Shelf, while the deeper portion of the Arctic Ocean is divided into two basins (both over 4000 meters deep) by the Lomonosov Ridge. In an attempt to retain some of the dynamical effects caused by these large bathymetric variations the model includes variable depth.

It is likely that the density variations in the Arctic Ocean effect the flow. For example a full treatment of the movement in the Atlantic layer (Coachman and Barnes 1963) will certainly require a baroclinic model. On the other hand there are some actual current measurements from the Arctic (Nikitin and Demyanov, 1965) (Galt, 1967) (Coachman, 1969) that indicate

a substantial barotropic, or depth independent component to the currents. This coupled with a consideration of the great increase in complexity required for variable density models suggests that for the initial numerical exploration a homogeneous or barotropic formulation be used.

The circulation in the Arctic is not well enough known to come up with an accurate appraisal of the significance of frictional forces. It seems likely that near source-sink points lateral friction could effect the flow. Over the large area covered by the Siberian Shelf it is quite possible that bottom friction might also be significant. Accordingly both lateral and bottom friction were included in the model and it was anticipated that some range of frictional parameters would be investigated to test for significance.

To develop a model with the characteristics described above the following integrated form of the equations of motion are used:

$$\frac{Du}{Dt} - fv = -\frac{1}{\rho} \frac{\partial P}{\partial x} + K \nabla^2 u - \frac{Ru}{h} + \frac{\tau_x}{\rho h} \quad (1)$$

$$\frac{Dv}{Dt} + fu = -\frac{1}{\rho} \frac{\partial P}{\partial y} + K \nabla^2 v - \frac{Rv}{h} + \frac{\tau_y}{\rho h} \quad (2)$$

Where the dependent variables u and v are the horizontal components of velocity which are independent of depth. The density, ρ , is a constant. τ_x and τ_y , the components of the wind stress, h , the depth, and f , the coriolis parameter, are functions of position. K and R are constants that specify the effectiveness of the horizontal and vertical frictional forces respectively.

In addition to these equations of motion we have the continuity equation:

$$\frac{\partial}{\partial x} (hu) + \frac{\partial}{\partial y} (hv) = 0 \quad (3)$$

A transport stream function is introduced such that:

$$\begin{aligned} -hu &= \frac{\partial \psi}{\partial y} \\ hv &= \frac{\partial \psi}{\partial x} \end{aligned} \quad (4)$$

The pressure can be eliminated from equations (1) and (2) and after some manipulation the following vorticity equation is obtained:

$$\begin{aligned} \frac{\partial \xi}{\partial \tau} - (\nabla \times \psi \vec{k}) \cdot \nabla \left(\frac{\xi + f}{h} \right) \\ = K \nabla^2 \xi - \frac{R}{h} \left[\xi + \nabla \psi \cdot \nabla \left(\frac{1}{h} \right) \right] + \nabla \times \left(\frac{\vec{\tau}}{\rho h} \right) \end{aligned} \quad (5)$$

where:

$$\xi = \frac{\partial v}{\partial x} - \frac{\partial u}{\partial y}$$

$$\nabla = \vec{i} \frac{\partial}{\partial x} + \vec{j} \frac{\partial}{\partial y}$$

$$\vec{\tau} = \tau_x \vec{i} + \tau_y \vec{j}$$

and \vec{i} , \vec{j} , \vec{k} are the unit vectors in the right handed x , y , z coordinate system.

From the above the following relationship between ξ and ψ is obtained:

$$\nabla \left(\frac{1}{h} \nabla \psi \right) = \xi \quad (6)$$

Equations (5) and (6) can now be solved for the vorticity and stream

function provided that the proper initial and boundary conditions are given. In particular the following must be specified:

- a) ψ - given within the region of interest at $t = 0$
- b) ψ - given on the boundary of the region for all time
- c) ξ - given within the region of interest at $t = 0$

Note that condition b) is equivalent to specifying the source-sink distribution around the edge of the model.

Equations (5) and (6) can be non-dimensionalized by introducing the following new variables:

$$\begin{aligned}
 t &= t' \left(\frac{1}{F} \right) & f &= f' F \\
 x &= x' \Delta & y &= y' \Delta \\
 h &= h' D & & \\
 \psi &= \psi' \psi_0 & & \\
 \tau &= \tau' \left(\frac{\rho F \psi_0}{\Delta} \right) & &
 \end{aligned} \tag{7}$$

Where the primed quantities are all non-dimensional, F is the average value of the Coriolis parameter, Δ is the finite difference grid spacing, D is the average depth of the model and ψ_0 is equal to the max range of stream function on the boundary of the model, or the maximum value expected for the wind driven portion of the flow, which ever is the most convenient.

Using the new variables defined above equations (5) and (6) become;

$$\begin{aligned}
 \frac{\partial \xi'}{\partial t} &= (\nabla \times \psi' \vec{k}) \cdot \nabla \left(\frac{\alpha \xi' + f'}{h'} \right) \\
 &= \beta \nabla^2 \xi' - \frac{\gamma}{h'} [\xi' + \psi' \cdot \nabla \left(\frac{1}{h'} \right)] + \nabla \times \left(\frac{\vec{\tau}}{h'} \right)
 \end{aligned} \tag{8}$$

$$\nabla\left(\frac{1}{h}, \nabla \psi'\right) = \xi' \quad (9)$$

Where:

$$\alpha = \frac{\psi_o}{\Delta^2_{DF}}$$

$$\beta = \frac{K}{\Delta^2_F}$$

$$\gamma = \frac{R}{DF}$$

These three non-dimensional parameters govern the character of the solution. For example setting $\alpha = 0$ removes the non-linear advective terms from the model. The size of β determines how important lateral friction is in the solution and γ scales the importance of bottom friction.

The finite difference grid that equations (8) and (9) are solved on is made up of a one dimensional array of $N \times M$ points. They are arranged as shown in figure 2. Grid points are numbered sequentially, left to right starting in the top row. This means that grid point in the neighborhood of the point L are given as shown in figure 2.

Two additional one dimensional arrays are used to specify the extent of the interior domain. These are integer arrays labeled IA and JA of dimension (M-2) and are defined so that a sweep of interior model points is obtained via the following algorithm.

```
DO 2 K=1, M-2
  I = IA(K)
  J = JA(K)
  DO 1 L = I, J
1 Statement on Interior Point (L)
2 Continue
```

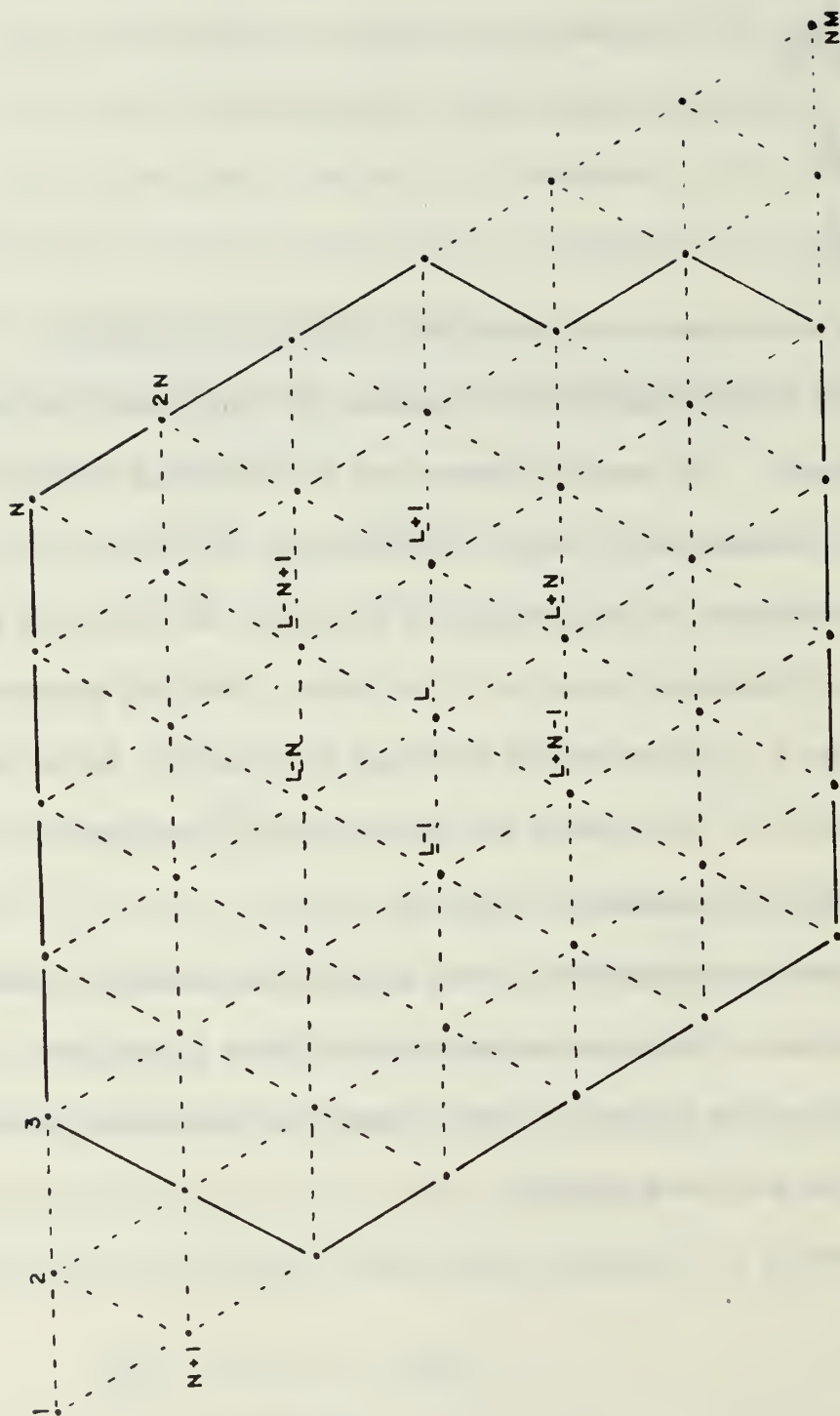


Figure 2. Grid pattern used in finite difference scheme and numbering system used for calculational molecule.

The depth in the model is specified in terms of an average depth and an array of deviations from this average. The amount of bathymetry to be used in any particular run is specified by a depth factor which is input at run time. The following depth variables are thus defined.

HM = average water depth

HFAC = depth factor

H (DIMENSIONED TO N x M) = array of depth deviations.

The actual depth used in any particular run is calculated with the following algorithm

DO 3 I = 1, NM

3 H(I) = HM + HFAC * H(I)

Obviously HFAC = 0 gives a constant depth model and HFAC = 1.0 includes all of the bathymetry. Any intermediate fraction is also possible if experimentation suggests such a case would be of interest.

To integrate equation (8) the three level Adams - Bashforth method is used. That is, writing equations (8) as:

$$\frac{\partial \xi'}{\partial t} = g'$$

we use:

$$\xi'(t' + \Delta t') = \xi'(t') + \left[\frac{3}{2} g'(t') - \frac{1}{2} g'(t' - \Delta t') \right] \Delta t' \quad (10)$$

To use this equation we must write g' in finite difference form. This will be done term by term starting with g' written as:

$$g' = (\nabla \times \psi') \cdot \nabla \left(\frac{\alpha \xi' + f'}{h'} \right) + \beta \nabla^2 \xi' - \frac{\gamma}{h'} \left[\xi' + \nabla \psi' \cdot \nabla \left(\frac{1}{h'} \right) \right] + \nabla \times \left(\frac{\vec{\tau}}{h'} \right) \quad (11)$$

The first term on the right hand side of equation (11) represents the net rate of potential vorticity advected into a unit area. To approximate this for the hexagon centered on the point L we write: (all quantities are non dimensional and primes have been omitted for simplicity)

$$\begin{aligned}
 (\nabla \times \vec{\psi}) \cdot \nabla \left(\frac{\alpha \xi + f}{h} \right) &= \frac{2}{3\sqrt{3}} [(\psi_{L-N+1} - \psi_{L+1}) \left(\frac{PV_{L-N+1} + PV_{L+1}}{2} \right) \\
 &+ (\psi_{L-N} - \psi_{L-N+1}) \left(\frac{PV_{L-N} + PV_{L-N+1}}{2} \right) + (\psi_{L-1} - \psi_{L-N}) \left(\frac{PV_{L-1} + PV_{L-N}}{2} \right) \\
 &+ (\psi_{L+N-1} - \psi_{L-1}) \left(\frac{PV_{L+N-1} + PV_{L-1}}{2} \right) + (\psi_{L+N} - \psi_{L+N-1}) \left(\frac{PV_{L+N} + PV_{L+N-1}}{2} \right) \\
 &+ (\psi_{L+1} - \psi_{L+N}) \left(\frac{PV_{L+1} + PV_{L+N}}{2} \right)] \quad (12)
 \end{aligned}$$

Where:

$$PV_I = (C1)(\xi_I) + f_I$$

and

$$C1 = \alpha = \frac{\psi_0}{\Delta_{DF}^2}$$

The second term on the right hand side of equation (11) represents the diffusion of vorticity horizontally and in finite difference form becomes:

$$\begin{aligned}
 \beta \nabla^2 \xi &= (C2) [\xi_{L+1} + \xi_{L-N+1} + \xi_{L-N} + \xi_{L-1} \\
 &+ \xi_{L+N-1} + \xi_{L+N} - (6)\xi_L] \quad (13)
 \end{aligned}$$

where

$$C2 = \frac{2\beta}{3} = \frac{2K}{3\Delta_{DF}^2}$$

the third term on the right hand side of equation (11) represents the

dissipation of vorticity through bottom friction and is written as:

$$\begin{aligned}
 \frac{\gamma}{h} \left[\xi + \nabla \psi \cdot \nabla \left(\frac{1}{h} \right) \right] = & \left(\frac{C3}{h_L} \right) \left\{ \xi_L + \left(\frac{1}{4} \right) [(\psi_{L+1} - \psi_{L-1}) \right. \\
 & + \left(\frac{1}{2} \right) (\psi_{L-N+1} - \psi_{L+N-1} - \psi_{L-N} + \psi_{L+N})] \\
 & \left[\frac{1}{h_{L+1}} - \frac{1}{h_{L-1}} + \left(\frac{1}{2} \right) \left(\frac{1}{h_{L-N+1}} - \frac{1}{h_{L+N-1}} - \frac{1}{h_{L-N}} + \frac{1}{h_{L+N}} \right) \right] \\
 & + \left(\frac{3}{8} \right) [\psi_{L-N+1} - \psi_{L+N-1} + \psi_{L-N} - \psi_{L+N}] \\
 & \left. \left[\frac{1}{h_{L-N+1}} - \frac{1}{h_{L+N-1}} + \frac{1}{h_{L-N}} - \frac{1}{h_{L+1}} \right] \right\}
 \end{aligned} \tag{14}$$

where:

$$C3 = \gamma = \frac{R}{DF}$$

The last term on the right hand side of equation (11) is the torque added per unit time by wind stress. This is assumed constant in time and calculated only once at the beginning of the program using the following finite difference form.

$$\begin{aligned}
 \nabla \times \left(\frac{\vec{\tau}}{h} \right) = & \frac{1}{2} \left\{ \left(\frac{G2}{h} \right)_{L+1} - \left(\frac{G2}{h} \right)_{L-1} \right\} \\
 & - \left(\frac{1}{\sqrt{3}} \right) \left\{ \left(\frac{G1}{h} \right)_{L-N+1} - \left(\frac{G1}{h} \right)_{L+N} + \left(\frac{G1}{h} \right)_{L-N} - \left(\frac{G1}{h} \right)_{L+N-1} \right\}
 \end{aligned} \tag{15}$$

Where G1 is the component of the wind stress in the direction from L to L + 1 and G2 is the component of the wind stress in a direction 90 degrees to the left of G1.

Equations (12) through (15) are used in equation (11) which in turn is used in the time integration scheme defined in equation (10). Once the vorticity has been obtained for a new time step equation (9) is solved by a

successive overrelaxation technique.

The algorithm used is a slight modification of the scheme suggested by Winslow (1961). The scheme used is as follows:

A residual is calculated:

$$\begin{aligned}
 \text{RES} &= \nabla \left(\frac{1}{h} \nabla \psi \right) - \xi \\
 &= \left(\frac{4}{3} \right) \left\{ \frac{\psi_{L+1}}{(h_{L+1} + h_L)} + \frac{\psi_{L-N+1}}{(h_{L-N+1} + h_L)} + \frac{\psi_{L-N}}{(h_{L-N} + h_L)} \right. \\
 &\quad \left. + \frac{\psi_{L-1}}{(h_{L-1} + h_L)} + \frac{\psi_{L+N-1}}{(h_{L+N-1} + h_L)} + \frac{\psi_{L+N}}{(h_{L+N} + h_L)} - \psi_L (\text{HFAC}_L) - \xi_L \right\}
 \end{aligned} \tag{16}$$

where:

$$\begin{aligned}
 \text{HFAC}_L &= \left(\frac{1}{h_{L+1} + h_L} \right) + \left(\frac{1}{h_{L-N+1} + h_L} \right) + \left(\frac{1}{h_{L-N} + h_L} \right) \\
 &\quad + \left(\frac{1}{h_{L-1} + h_L} \right) + \left(\frac{1}{h_{L+N-1} + h_L} \right) + \left(\frac{1}{h_{L+N} + h_L} \right)
 \end{aligned}$$

The residual is then normalized using the coefficient of ψ_L in equation (16), i.e.,

$$d\psi = \left(\frac{4}{3} \right) \left(\frac{1}{\text{HFAC}_L} \right) \text{RES}$$

and the relaxation is then given by:

$$\psi_L = \psi_L + (R)d\psi_L \tag{17}$$

A number of tests were run to estimate the optimal value for R and over a wide range of cases a value of 1.48 was indicated. This value was then used throughout the modeling efforts reported here.

The typical experiment anticipated for the model will be to apply some

stress field to a static ocean. The model ocean will then spin-up, or develop a circulation pattern that will generally approach a steady state providing an appropriate balance of torque is possible and that the applied stress field is steady. The time dependent development of the steady state circulation and to some extent the final flow pattern will depend on the characteristics of the planetary waves that make up the transients in the model. For this reason it is of some interest to look at the propagation characteristics of these waves within the model and to estimate the errors introduced by the finite difference scheme.

To estimate how the model transients will respond a simple, free, linear Rossby wave will be considered. For this case the vorticity equation (5) reduces to:

$$\frac{\partial}{\partial \tau} \left(\frac{1}{h} \nabla^2 \psi \right) = -h \mathbf{v} \cdot \nabla \left(\frac{f}{h} \right) \quad (18)$$

A wave form of the solution is assumed and near by values used in the computational molecule (Fig. 2) taken as follows:

$$\begin{aligned} \psi_L &= \psi_0 \epsilon^{i(kx + ly - \omega t)} \\ \psi_{L+1} &= \epsilon^{ik\Delta} \psi_L \\ \psi_{L-N+1} &= \epsilon^{\frac{i\Delta}{2} (k + \sqrt{3}l)} \psi_L \\ \psi_{L-N} &= \epsilon^{\frac{i\Delta}{2} (-k + \sqrt{3}l)} \psi_L \\ \psi_{L-1} &= \epsilon^{-ik\Delta} \psi_L \end{aligned} \quad (19)$$

$$\psi_{L+N-1} = \epsilon^{\frac{i\Delta}{2}(-k-\sqrt{3}\ell)} \psi_L$$

$$\psi_{L+N} = \epsilon^{\frac{i\Delta}{2}(k-\sqrt{3}\ell)} \psi_L$$

Where x and y refer to position in a right handed co-ordinate system superimposed on the finite difference grid with the positive x -axis in the direction from L to $L + 1$. It can also be assumed with no loss of generality that the x and y axes are directed east and north respectively. This then gives:

$$\frac{\partial f}{\partial x} = 0 ; \quad \frac{\partial f}{\partial y} = \beta^* \quad (20)$$

To obtain a reasonable estimate of the phase velocity for the Rossby waves in the model the time differencing can be assumed exact and the depth assumed constant. Using equations (19) and (20) with the finite difference forms given in equations (12) and (13), the vorticity equation given in (18) becomes, after some simplification.

$$-i\omega \frac{4\psi_L}{3h\Delta^2} [\cos k\Delta + 2 \cos(\frac{\sqrt{3}\ell\Delta}{2}) \cos(\frac{k\Delta}{2}) - 3]$$

$$= \frac{-2i\beta^*}{\Delta} [\sin k\Delta + \sin(\frac{k\Delta}{2}) \cos(\frac{\sqrt{3}\ell\Delta}{2})]$$

Which gives

$$\omega = \frac{\beta^*\Delta}{2} \left[\frac{\sin(k\Delta) + \sin(\frac{k\Delta}{2}) \cos(\frac{\sqrt{3}\ell\Delta}{2})}{\cos(k\Delta) + 2 \cos(\frac{k\Delta}{2}) \cos(\frac{\sqrt{3}\ell\Delta}{2}) - 3} \right]$$

For small Δ the trig functions can be expanded using small angle approximations.

This gives:

$$\omega = -\beta^* \left[\frac{k - \frac{1}{8} (k^3 + k\ell^2) (\Delta^2)}{k^2 + \ell^2 + \left(\frac{k^4}{18} + \frac{k^2 \ell^2}{8} \right) (\Delta^2)} \right]$$

And from this dispersion relation it can easily be seen that the x component of the phase velocity is:

$$C_x = \frac{\omega}{k} = -\beta^* \left[\frac{1 - \frac{1}{8} (k^2 + \ell^2) (\Delta^2)}{\ell^2 + k^2 + \left(\frac{k^4}{18} + \frac{k^2 \ell^2}{8} \right) (\Delta^2)} \right] \quad (21)$$

Clearly as Δ goes to zero this goes to the exact form

$$C_x = -\frac{R^*}{k^2 + \ell^2}$$

and the error term is second order in Δ . This then suggests that the transient wave solutions that develop in the model will be accurately represented to second order.

The actual fortran program used for the model and an explanation of the input data required is given in an appendix.

Section III - Preliminary Results

The characteristics of the model described in the last section have been investigated in a series of tests designed to check out the numerical properties of the solutions. In a number of cases it was also possible to illustrate the physical significance that the processes represented might have on the circulation in the Arctic Ocean.

The first test was to check the part of the program that handled the



Figure 3. Configuration of the model used to check out the relaxation of the stream function.

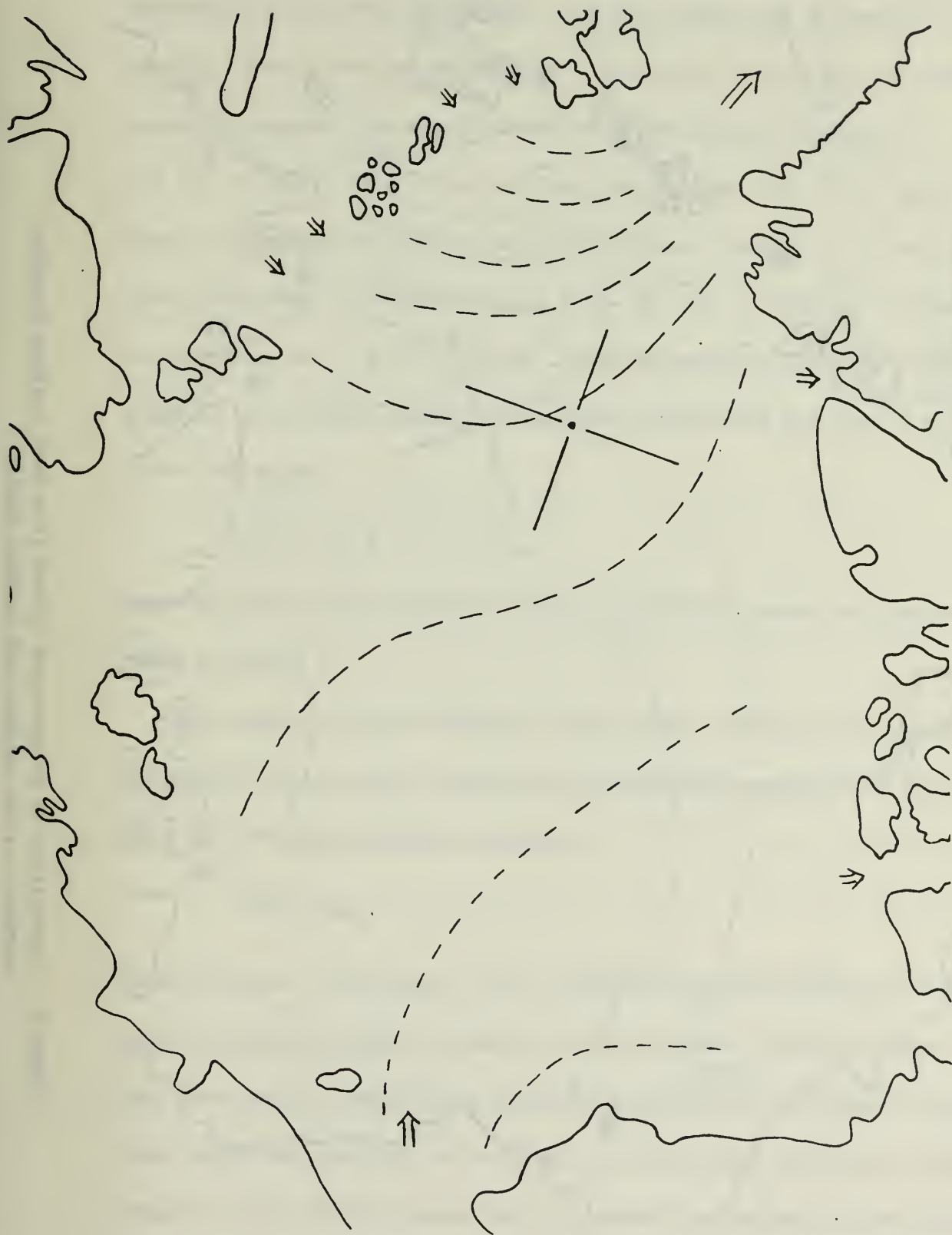


Figure 4. Streamlines of source-sink driven flow with zero vorticity in the interior and uniform depth.



Figure 5. Streamlines of source-sink driven flow with uniform negative vorticity in the interior and uniform depth.

relaxation of the stream function. A basin shape was chosen that roughly covered the deeper portion of the Arctic Ocean (Fig. 3). Representative source-sink distributions were specified as follows:

$2 \times 10^6 \text{ m}^3 \text{ sec}^{-1}$ flow in across the Chukchi Sea, $7 \times 10^6 \text{ m}^3 \text{ sec}^{-1}$ flow in spread out on either side of Franz Josef Land, $1 \times 10^6 \text{ m}^3 \text{ sec}^{-1}$ flow out through M'Clure Strait, $1 \times 10^6 \text{ m}^3 \text{ sec}^{-1}$ flow out into the Lincoln Sea, and $7 \times 10^6 \text{ m}^3 \text{ sec}^{-1}$ flow out into the East Greenland current. With a flat bottom the equations governing the flow in the interior reduce to:

$$\nabla^2 \psi = 0$$

Solving this for the specified boundary conditions gives the flow indicated in Figure 4.

The next test case introduced some finite vorticity into the above equation. For the initial testing this was simply specified as a constant. Thus the governing equation becomes:

$$\nabla^2 \psi = h\xi_0$$

This obviously corresponds to the artificial case where equation 8 has gone to a steady-uniform solution for the vorticity. Although this is not very realistic the results are interesting and shown in Figure 5 for the case where the vorticity in the flow is constant and negative as one might expect to get from the stress field developed by the polar easterlies. Circulation resembling the Beaufort Gyre develops. Qualitatively the results show a striking resemblance to the very viscous solution

for ice drift presented by Campbell (1965, Fig. 7c,d).

The next set of experiments with the model were to check out the time dependent vorticity equation (8) in conjunction with relaxation of the stream function (Eq. 9). To do this a basin roughly the shape of the Arctic was specified. Non-linear terms and bottom friction were not included ($\alpha = \gamma = 0$). A uniform negative stress curl was applied to the water that was initially at rest. The Coriolis parameter was assumed constant.

For the first series of runs made on this configuration the depth was assumed constant. Under these conditions the model would spin-up forming a symmetric clock-wise circulation pattern. The steady state solution represented a balance between the torque added by the wind and that which was lost through lateral friction. The magnitude of the steady state solution and the spin-up time of the model depended on the magnitude of the frictional coefficient (β) that was used. It is interesting to note that for this series the vorticity equation reduces to:

$$\frac{\partial \xi}{\partial t} = \beta \nabla^2 \zeta + \frac{1}{h} (\nabla \times \tau) \quad (22)$$

With a steady wind stress this equation has no wave solutions and the appropriate von Neumann type stability condition (Richtmyer and Morton, 1967) will be of the form:

$$\beta t \leq \text{constant} \approx \frac{1}{4} \quad (23)$$

(Assuming the Adams-Bashforth scheme is used for time differencing.)

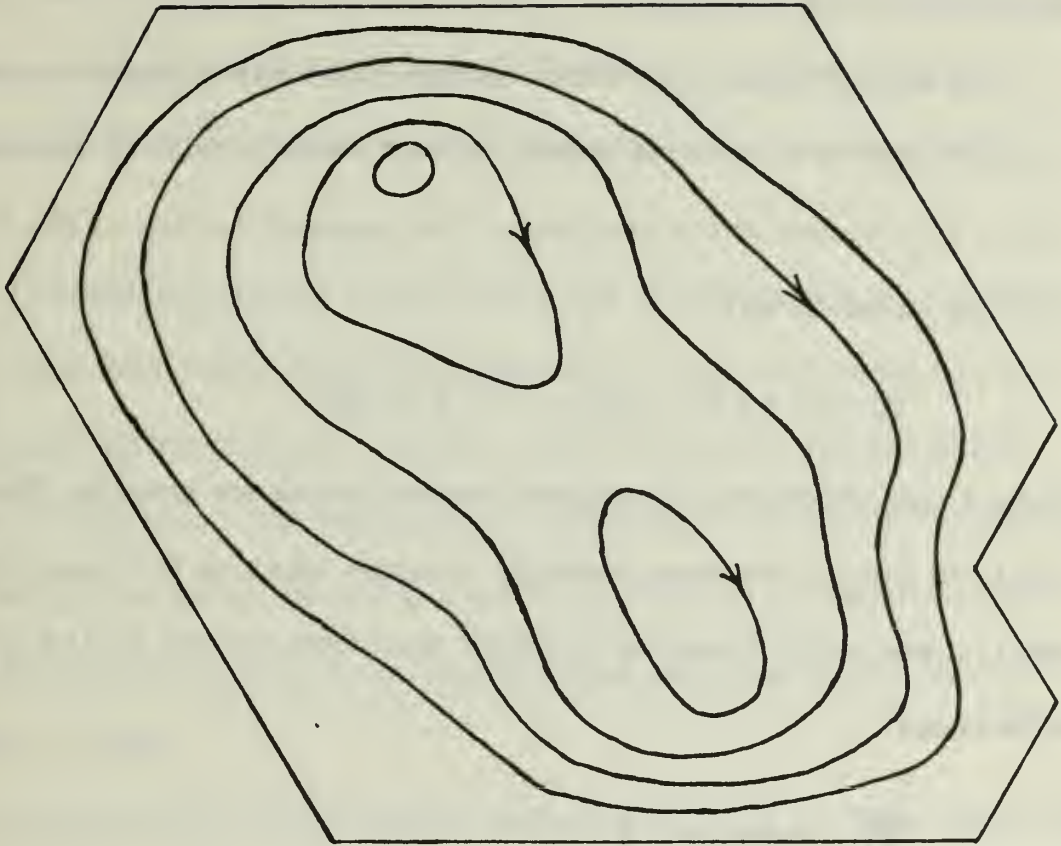


Figure 6. Streamlines of flow driven by uniform stress curl in an irregular shaped ocean with a central ridge. (The ridge runs from top to bottom in the figure.)

Where t is the non-dimensional time step in half pendulum days. This is relatively weak restriction in that with more or less realistic geophysical parameters time steps of a number of days are possible. This was confirmed with the model.

The second series run on this configuration was designed to test the models response to variable depth. In this series a ridge of smooth profile was placed across the basin. The appropriate form of the vorticity equation was

$$\frac{\partial \xi}{\partial t} - f(\nabla \times \psi \vec{k}) \cdot \nabla \left(\frac{1}{h}\right) = \beta \nabla^2 \xi + \nabla \times \left(\frac{\tau}{h}\right) \quad (24)$$

Under these conditions topographic Rossby waves are possible (Veronis, 1966) and the von Neumann stability criterion takes on the more restrictive form: (Once again assuming an Adams-Bashforth scheme for the time differences)

$$\frac{Ct}{\Delta f} \leq \text{constant} \approx \frac{1}{2} \quad (25)$$

Where C is the phase speed of the topographic Rossby waves. This general behavior was again confirmed by the model.

In this series the spin-up of the model begins as before, but the variable depth acts in many ways analogously to a variable F in a flat bottom ocean and western boundary type currents can develop. These stronger boundary currents develop not on the western side of the ocean basin as in Munk's model (Munk, 1950) but rather to the left of an observer looking from deep to shallow water. Figure 6 shows a typical solution

for this series. The ridge is seen to divide the flow into two cells with regions of intensified currents in each half.

During the initial spin-up for this series transient wave patterns were seen to propagate along the ridge. It is quite likely that the real time dependent stress fields applied to the Arctic ocean will result in transients of this form being propagated along the Lomonosov Ridge (Fig. 1).

An additional series of tests were run to investigate the interaction of source-sink terms with the bathymetry and the formulation used to represent bottom friction. For this series the stress applied at the surface was zero. The source-sink distribution was simply to have flow in through the Bering Straits and out through the East Greenland area. The bathymetry was again the smooth ridge described in the previous series of tests.

The first test in this series assumed $\alpha = \beta = \gamma = 0$. Thus there was no friction, or non-linear terms. The appropriate form of the vorticity equation that was:

$$\frac{\partial \xi}{\partial t} - (\nabla \times \psi \vec{k}) \cdot \nabla \left(\frac{f}{h} \right) = 0 \quad (26)$$

This equation shows the interesting result that the only steady flow possible is when the stream lines are parallel to lines of constant f/h . Thus the steady-state flow can not cross the ridge and any source-sink distribution that demands cross ridge flow will not lead to a steady circulation. The numerical model shows these characteristics with

circulation continuing to increase with time. A strong negative (clock-wise) circulation builds up on the in-flow side of the ridge and a corresponding positive circulation develops on the outflow side of the ridge. This is similar to the effect one might get if the water simply piled up on the in-flow side and drained out on the out-flow side satisfying the overall continuity requirements for the ocean but with minimum cross-ridge flow.

This has an important implication for the circulation in the Arctic. If the source-sink component of the flow is to be barotropic and geostrophic then flow can not cross the Lomonosov ridge. This means that continuity must be satisfied separately for both basins in the Arctic. There will be a strong tendency for flow that enters on the Canadian side of the Arctic to exit on the same side. Field data from the Arctic suggest that this may in fact be the case (Coachman, 1970). Thus one might expect that flow through the Bering Straits and the Canadian Archipelago should be strongly correlated.

The next runs in this series included the non-linear terms and lateral friction which gave the following governing vorticity equation:

$$\frac{\partial \xi}{\partial t} - (\nabla \times \psi \vec{k}) \cdot \nabla \left(\frac{\alpha \xi + f}{h} \right) = \beta \nabla^2 \xi \quad (27)$$

For this case both frictional and non-linear boundary layers are present with cross ridge flow taking place and a steady-state solution is possible. For all reasonable values of α and β the interior of the flow is still essentially geostrophic and the cross ridge flow takes place in boundary layers

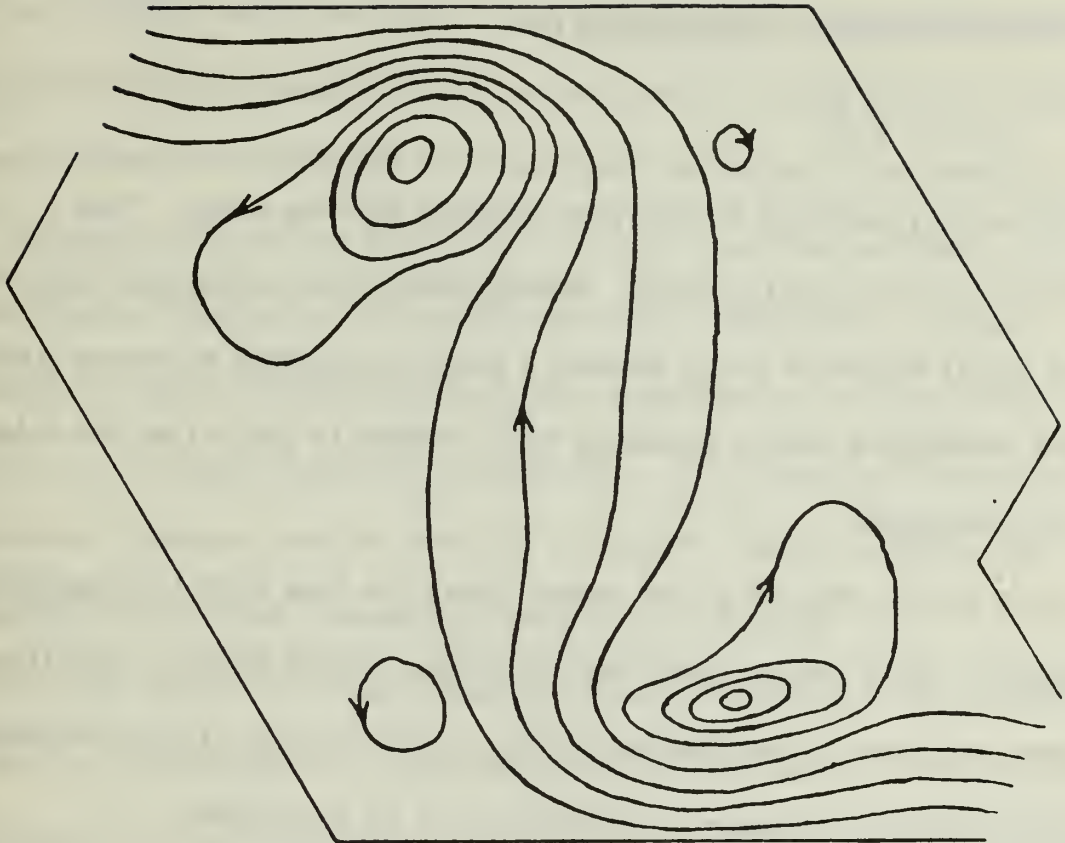


Figure 7. Streamlines of flow driven by a simple source-sink distribution for an irregular shaped ocean with a central ridge. (The ridge runs from the top to the bottom in the figure.)

where the ridge intersects the sides of the basin. (Fig. 7)

A final case run in this series included the bottom friction terms. It can be anticipated that bottom friction would be effective in causing cross bathymetry flow. In particular the

$$\frac{\gamma}{h} \nabla \psi \cdot \nabla \left(\frac{1}{h} \right)$$

term will have a tendency to turn flow towards shallow water. This is in fact what the model showed. Steady state flows resembled figure 7 for very small values of γ and showed a smooth transition to stream line patterns resembling simple hydraulic flow (similar to Fig. 4) as the value of γ was increased.

In the deeper interior of the Arctic Ocean the flow must be essentially geostrophic, but it seems likely that frictional effects must be significant over large portions of the Siberian shelf. In the vicinity of the Lomonosov Ridge both friction and non-linear effects may be significant.

Section IV - Future Model Plans

The next stages in the development and use of this model are well under way at the time of this writing.

The first extension is to use the model with greatly increased resolution and the actual bathymetric variation of the Arctic basins. With this configuration realistic source-sink distributions are investigated. A wind stress field obtained from Felezenbaum's pressure data (Felezenbaum, 1958) is used to drive the flow and a number of runs are

anticipated to investigate the effects of variations in α , β and γ .

The next series of tests will use the same basic model configuration but the stress field will be obtained by applying Felezenbaum's pressure data to Campbell and Rasmussen's (1971) ice model and then using the stress field from the bottom of the ice to drive the ocean model. Again a series of runs are anticipated to investigate variations in parameters.

Another series of runs is planned for the model that will have even higher spacial resolution and definitions of the bathymetry. In this series the ocean will be driven by a time dependent wind stress field that is made up of random frequency components. The dependent variables at a number of locations will be spectral analyzed with the intension of obtaining normal mode frequencies for the Arctic basins.

The next stage in the development of model exploration for the Arctic will be the formulation of a baroclinic model. The first set of experiments anticipated for this formulation will be the investigation of the dynamics associated with the circulation of the Atlantic Layer (Coachman and Barnes, 1963).

References

- Aagaard, Knut, (1966). The East Greenland Current North of the Denmark Strait. Ph.D. Thesis, Dept. of Ocean. Univ. of Wash. 83 pg.
- Campbell, W. J., (1955). The Wind Driven Circulation of Ice and Water in a Polar Ocean. Jour. Geophys. Res. 70(14): 3279-3301.
- Campbell, W. J. and L. A. Rasmussen, (1971). Personal communication.
- Coachman, L. K., (1969). Physical oceanography in the Arctic Ocean: 1968. Arctic 22(3): 214-224.
- (1970). Towards an operational technology for the Arctic Ocean. Arctic Inst. N-Am. workshop Oct. 12, 13 and 14. Arlington, Va.
- , and C. A. Barnes (1961). The contribution of the Bering Sea water to the Arctic Ocean. Arctic 14(3): 147-161.
- , and C. A. Barnes (1963). The movement of Atlantic water in the Arctic Ocean. Arctic 16(1):9-16.
- Felzenbaum, A. I. (1958). The theory of the steady drift of ice and the calculation of the long period mean drift in the central part of the Arctic basin. Problems of the North, 2, 5-15, 13-44.
- Galt, J. A. (1967). Current measurements in the Canadian Basin of the Arctic Ocean. Summer 1955. Univ. of Wash., Dept of Ocean., Tech. Report No. 184.
- Holland, William R. (1967). On the wind-driven circulation in an ocean with bottom topography. Tellus 19(4): 582-599.
- Maykut, Gary A. and Norbert Untersteiner. (1971). Some results from a time dependent thermodynamic model of sea ice. Jour. Geophys. Res. 76(6): 1550-1575.
- Muench, R. D. (1971). The physical oceanography of the Northern Baffin Bay region. Arctic Inst. N-Amer. Baffin Bay - North Water Project Sc. Rep. No. 1.
- Munk, W. H. (1950). On the wind-driven ocean circulation. Jour. of Met. 7(2): 79-93.
- Nikitin, M. M. and N. I. Dem'yanov (1965) O glubinnikh techeniyakh Arkticheskogo Passeina. Okeanologiya 5(2):261-263.

- Richtmyer, R. D. and K. W. Morton (1957). Difference methods for initial-value problems. Interscience pub. Inc., New York. 237 pages.
- Sadourny, Robert, Akio Atakawa and Yale Mintz (1967). Integration of the non-divergent barotropic vorticity equation with an icosahedral-hexagonal grid for the sphere. Dept. of Met., U.C.L.A., Num. Simulation of Weather and Climate, Tech. Rept. No. 2.
- Thorndike, A. (1971) personal communication AIDJEX planning conference, June 1971 Lake Wilderness Conference Center, Washington.
- Untersteiner, N. and J. O. Fletcher (1971). AIDJEX planning conference introduction AIDJEX Bulletin No. 9. Arctic-Ice-Dyn-Joint Experiment, Div. of Marine Res. Univ. of Wash., Seattle.
- Veronis, George. (1966). Rossby waves with bottom topography. Jour. Mar. Res. 24(3): 388-394.
- Williamson, David L. (1970). Integration of the barotropic vorticity equation on a spherical geodesic grid. Tellus, 20(4): 624-653.
- Winslow, Alan M. (1967). Numerical solution of the quasilinear Poisson equation in a non-uniform triangular mesh. Jour. Comp. Phy. 1(2):149-172.

Appendix - Use of Computer Program

The ocean model program has been written in FORTRAN - IV and a listing of the program is included in the end of this appendix. To use the program an appropriate data deck must be placed after the program. The composition of the data deck must be as follows:

- 1) N, M, NB FORMAT (3I3) - this is a single card where N and M are the dimensions of the grid system (ref. Fig. 2) and NB is the number of boundary points.
- 2) IA FORMAT (2I3) - this is a grid number list of the first interior point of each line down the left hand side of the model.
- 3) JA FORMAT (2I3) - this is a grid number list of the last interior point of each line down the right hand side of the model.
- 4) LV, BLANK FORMAT (2I1) - this is a single card with the code to be used in the graphical out put of the program. (Ref. subroutine GRAOUT)
- 5) HM, FAC FORMAT (2F6.1) - this is a single card where HM is the reference depth and FAC is the fraction of the bathymetry that is desired in the model.
- 6) H FORMAT (12F6.4) - this is a set of cards that has the normalized depth variation for each grid point.
- 7) F FORMAT (12F6.4) - this is a set of cards that has the normalized values of the Coriolis parameter for each grid point.

- 8) I FORMAT (13) - this is a single card with the exponential part of the values to be used for the wind stress.
- 9) GI FORMAT (12F5.3) - this is a set of cards with the significant figures part of the wind stress in the direction of the positive axis, i.e. from point L to L + 1 (Ref. Fig. 2).
- 10) G2 FORMAT (12F5.3) - this is a set of cards with the significant figures part of the wind stress in the direction 90° to the left of the positive axis.
- 11) IBC FORMAT (6(6I1, I3)) - this is a set of cards that contains the information required to calculate boundary values of vorticity. For each boundary point a six digit code and the grid number are given. The six digit code refers to the neighboring points in a counter clock-wise order starting with L + 1. The following code is used:
0 - exterior point, 1 - interior point (free slip B.C.), 2 - interior point (no slip B.C), 3 - boundary point along streamline, 4 - boundary point across a streamline. Boundary points at sources are not included in the IBC list.
- 12) C1, C2, C3, DT, TOUT, TMAX, R, CON, 1PUNCH FORMAT(6E10.3, F4.2, E10.3, 12) - this is a single card that contains the run parameters. C1, C2 and C3 are defined in section two of this report. DT is the time step. TOUT is the time interval at which output of the dependent variables is desired. TMAX is the maximum time the model is to run. R is the SOR parameter to be used for the relaxation of the

stream function. CON is the absolute convergence limit to be used for the relaxation of the stream function. IPUNCH is a flag that should be non-blank if the final values for the dependent variables are required as a source deck for future runs.

- 13) S FORMAT (6E12.5) - this is a set of cards that contain the initial values for the stream function at each grid point.
- 14) V FORMAT(6E12.5) - this is a set of cards that contain the initial values for the vorticity at each grid point.
- 15) G1 FORMAT(6E12.6) - this is a set of cards that contain the initial values of the local time rate of change of the vorticity at time $-(-DT)$.

```

00011 NUMERICAL OCEAN MODEL PROGRAM - DEVELOPED MAY 1971 J. A. GALT
00012
00013
00014 ALL OF THE ARRAYS USED IN THE PROGRAM ARE DIMENSIONED HERE. IA(M2)
00015 AND JA(M2) SPECIFY THE SHAPE OF THE BASIN. H(NM), F(NM) AND T(NM)
00016 ARE USED FOR THE INDEPENDENT VARIABLES WATER DEPTH, CORIOLIS
00017 PARAMETERS AND WIND STRESS CURV RESPECTIVELY. THE DEPENDENT
00018 VARIABLES ARE ASSOCIATED WITH S(NM) FOR THE STREAM FUNCTION AND
00019 V(NM) FOR THE VORTICITY. G1(NM) AND G2(NM) ARE CALCULATIONAL
00020 ARRAYS USED FOR TEMPORARY STORAGE AND LV(20) AND LO((2*N+M-2)*M)
00021 ARE USED FOR THE OUTPUT OF ARTS DATA. IBC(7,NB) IS AN ARRAY
00022 THAT CONTAINS THE COEFFICIENTS NEEDED TO CALCULATE BOUNDARY VALUES
00023 FOR THE VORTICITY. RES(NM) IS AN ARRAY USED IN THE VARIABLE DEPTH
00024 PART OF THE STREAM FUNCTION RELAXATION. LA(6) IS A STORAGE ARRAY
00025 USED DURING THE CALCULATION OF VORTICITY ON THE BOUNDARY POINTS.
00026 HC1(NM) AND HC2(NM) ARE COEFFICIENT ARRAYS USED IN THE
00027 CALCULATION OF BOTTOM STRESS.
00028
00029 DIMENSION IA(5),JA(5),H(49),F(49),T(49),G1(49),G2(49),LV(20),
00030 LO(133),IBC(7,18),RES(49),V(49),S(49),LA(6),
00031 HC1(49), HC2(49)
00032
00033 THE PROGRAM STARTS BY READING IN THE SIZE OF THE MAJOR ARRAY
00034 WHICH WILL BE N BY M POINTS AND THE NUMBER OF BOUNDARY
00035 POINTS NB
00036
00037 READ(5,100) N,M,NB
00038 FORMAT(3I3)
00039
00040 SIZE PARAMETERS ARE NOW CALCULATED. NM IS THE TOTAL NUMBER
00041 OF GRID POINTS AVAILABLE TO THE DEPENDENT VARIABLES. NOUT
00042 IS THE NUMBER OF POINTS USED IN THE OUTPUT ARRAY. AND, M2
00043 IS THE SIZE OF THE ARRAYS USED TO SPECIFY THE BASIN SHAPE.
00044
00045 NM = N*M
00046 NOUT = (2*N+M-2)*M
00047 M2 = M-2
00048
00049 THE ARRAYS THAT SPECIFY THE BASIN SHAPE ARE NOW READ IN
00050
00051 READ(5,101) IA
00052 READ(5,101) JA
00053 FORMAT(20I3)
00054
00055 THE ALPHA CODE USED IN THE OUTPUT ARRAYS IS READ IN
00056
00057 READ(5,102) LV,BLANK
00058 FORMAT(21A1)
00059
00060
00061
00062
00063
00064
00065
00066
00067
00068
00069
00070
00071
00072
00073
00074
00075
00076
00077
00078
00079
00080
00081
00082
00083
00084
00085
00086
00087
00088
00089
00090
00091
00092
00093
00094
00095
00096
00097
00098
00099
00100
00101
00102
00103
00104
00105
00106
00107
00108
00109
00110
00111
00112
00113
00114
00115
00116
00117
00118
00119
00120
00121
00122
00123
00124
00125
00126
00127
00128
00129
00130
00131
00132
00133
00134
00135
00136
00137
00138
00139
00140
00141
00142
00143
00144
00145
00146
00147
00148

```

```

103 WRITE(6,103)
    FORMAT(1H1,22H NUMERICAL OCEAN MODEL ///,
    19H THE BASIN SHAPE IS ///),
    DO 2 K = 1,M2
    I = IA(K)
    J = JA(K)
    DO 1 L = I,J
    H(L) = FLOAT(L)
    CONTINUE
    CALL GRAOUT(LV,LO,NOUT,H,NM,IA,JA,M2,N,BLANK)
C
C THE REFERENCE DEPTH HM AND THE DEPTH FACTOR FAC ARE READ
C IN. AFTER THIS THE NORMALIZED DEPTH VARIATIONS ARE
C READ IN AND THE WORKING DEPTHS CALCULATED.
C
104 READ(5,104) HM,FAC
    FORMAT(2F6.1)
105 READ(5,105) H
    FORMAT(12F5.3)
20 DO 20 I = 1,NM
    H(I) = 1.0+FAC*H(I)
    WRITE(6,106) HM,FAC
106 FORMAT(1H1,25H THE REFERENCE DEPTH IS = ,F8.2,7H METERS,/,
    22H THE DEPTH FACTOR IS = ,F6.3///)
E
107 WRITE(6,107)
    FORMAT(40H THE ARRAY OF NORMALIZED DEPTH VALUES IS ///)
108 WRITE(6,108) H
    FORMAT(12F8.3)
109 WRITE(6,109)
    FORMAT(// 18H BOTTOM TOPOGRAPHY //)
    CALL GRAOUT(LV,LO,NOUT,H,NM,IA,JA,M2,N,BLANK)
C
C THE NORMALIZED VALUES OF THE CORIOLIS PARAMETER ARE NOW READ IN
C
110 READ(5,110) F
    FORMAT(12F6.4)
111 WRITE(6,111)
    FORMAT(1H1,46H THE DISTRIBUTION OF THE CORIOLIS PARAMETER IS ///)
170 WRITE(6,170) F
    FORMAT(12F8.4)
    CALL GRAOUT(LV,LO,NOUT,F,NM,IA,JA,M2,N,BLANK)
C
C THE PROGRAM NOW READS IN TWO COMPONENTS OF THE NORMALIZED WIND
C STRESS. G1 GIVES ITS COMPONENT IN THE POSITIVE AXIS DIRECTION
C AND G2 GIVES ITS MAGNITUDE IN A DIRECTION 90 DEGREES TO THE LEFT
C THE STRESS HAS BEEN NONDIMENSIONALIZED USING  $T = (\rho H F S1/L)T^*$ .
C TO SAVE SPACE ON THE INPUT CARDS THE EXPONENT PART OF THE STRESS
C IS READ IN FIRST

```



```

C      DO 21 I = 1, NM
21      T(I) = 0.0
      READ(5,112) I
112      FORMAT(I3)
      FAC = 10.0**I
      READ(5,105) G1
      READ(5,105) G2
      DO 3 I = 1, NM
3      G1(I) = FAC*G1(I)/H(I)
      G2(I) = FAC*G2(I)/H(I)
      C
      C      HERE THE CURL OF T/H IS CALCULATED
      C
      AREA = 2.598376
      FAC1 = 1.0/SQRT(3.)
      DO 5 K = 1, M2
      I = IA(K)
      J = JA(K)
      DO 4 L = I, J
      L1 = L+1
      L2 = L-N+1
      L3 = L-N
      L4 = L-1
      L5 = L+N-1
      L6 = L+N
      T(L) = 0.5*(G2(L1)-G2(L4)-(G1(L2)-G1(L6)+G1(L3)-G1(L5))*FAC1)
      C
      C      WHILE IN THE LOOP RES(NM), HC1(NM) AND HC2(NM) ARE ALL CALCULATED
      C      FOR USE LATER IN THE RELAXATION OF THE STREAM FUNCTION AND THE
      C      BOTTOM STRESS TERM
      C
      FAC = H(L)
      RES(L) = 1.0/(FAC+H(L1))+1.0/(FAC+H(L2))+1.0/(FAC+H(L3))
      E      +1.0/(FAC+H(L4))+1.0/(FAC+H(L5))+1.0/(FAC+H(L6))
      HC1(L) = 0.25*(1./H(L1) - 1./H(L4) + 0.5*(1./H(L2) - 1./H(L5)
1      - 1./H(L3) + 1./H(L6)))
      HC2(L) = (1./H(L2) - 1./H(L5) + 1./H(L3) - 1./H(L6)) * (3./8.)
      C
      C      CONTINUE
      C      CONTINUE
      C      WRITE(6,180) THE DISTRIBUTION OF THE WIND STRESS CURL IS
4      5      FORMAT(IH1,45H)
180      WRITE(6,173) T
      WRITE(6,118)
      CALL GRAOUT(LV,LO,NOUT,T,NM,IA,JA,M2,N,BLANK)
      C
      C      THE ARRAY THAT CONTAINS THE INFORMATION NEEDED TO CALCULATE
      C      THE BOUNDARY VALUES FOR THE VORTICITY IS NOW READ IN.

```



```

C      113      READ(5,113) IBC
C      FORMAT(6I1,13)
C
C      RUN PARAMETERS ARE READ IN AT THIS POINT. C1 IS THE
C      NON-LINEAR COEFFICIENT S1/FDL**2, C2 IS THE FRICTIONAL
C      COEFFICIENT 2K/3FL**2, C3 IS THE BOTTOM STRESS
C      COEFFICIENT R/DF, DT IS THE NON-DIMENSIONAL TIME
C      STEP, TOUT IS THE MAXIMUM MODEL TIME, R IS THE
C      PRINTED OUT, TMAX IS THE RELATIVE CONVERGENCE FACTOR
C      RELAXATION PARAMETER, CON IS THE STREAM FUNCTION AND IPUNCH
C      FOR THE RELAXATION OF THE STREAM FUNCTION AND IPUNCH
C      IS A FLAG USED IF THE FINAL VALUE OF THE DEPENDENT
C      VARIABLES IS PUNCHED OUT AS A DATA DECK.
C
C      114      READ(5,114) C1,C2,C3,DT,TOUT,TMAX,R,CON,IPUNCH
C      FORMAT(6E10.3,F4.2,E10.3,I2)
C      WRITE(6,171)
C      171      FORMAT(1H1, 'THE RUN PARAMETERS C1,C2,C3,DT,TOUT,TMAX,R,CON AND
C      172      IPUNCH ARE: ')
C      WRITE(6,172) C1,C2,C3,DT,TOUT,TMAX,R,CON,IPUNCH
C      FORMAT(8E14.3, I6)
C
C      THE INITIAL VALUES FOR THE VORTICITY, STREAM FUNCTION AND
C      THE LOCAL CHANGE IN THE VORTICITY ONE TIME STEP BACK
C      ARE READ INTO THE PROGRAM
C
C      115      READ(5,115) S
C      READ(5,115) V
C      READ(5,115) G1
C      FORMAT(6E12.5)
C
C      THE TIME CONTROL IS STARTED NOW AND THE ACTUAL
C      CALCULATION OF THE PROGRAM BEGINS
C
C      ITER = 0
C      TIME = 0.0
C      CONTINUE
C      FAC = TIME/TOUT+0.01*DT
C      IF (FAC) 1
C      FAC = FLOAT(I)
C      FAC = TOUT*FAC
C      FAC = TIME-FAC
C      FAC = ABS(FAC)
C      DTERR = 0.1*DT
C      IF (FAC.GT.DTERR) GO TO 7
C
C      IN THIS SECTION THE DEPENDENT VARIABLES ARE PRINTED OUT

```



```

0241 L2 = L-N+1
0242 L3 = L-N
0243 L4 = L-1
0244 L5 = L+N-1
0245 L6 = L+N
0246
0247 HERE THE CONTRIBUTION FROM THE ADVECTION OF POTENTIAL
0248 VORTICITY IS CALCULATED
0249
0250 A1 = (C1*V(L1)+F(L1))/H(L1)
0251 A2 = (C1*V(L2)+F(L2))/H(L2)
0252 A3 = (C1*V(L3)+F(L3))/H(L3)
0253 A4 = (C1*V(L4)+F(L4))/H(L4)
0254 A5 = (C1*V(L5)+F(L5))/H(L5)
0255 A6 = (C1*V(L6)+F(L6))/H(L6)
0256 FAC = ((S(L2)-S(L1))*(A2+A1)+(S(L3)-S(L2))*(A3+A2)
0257 + (S(L4)-S(L3))*(A4+A3)+(S(L5)-S(L4))*(A5+A4)+(S(L6)-S(L5))
0258 * (A6+A5)+(S(L1)-S(L6))*(A1+A6))/(2.0*AREA)
0259
0260 THE CONTRIBUTION FROM THE DIFFUSION OF VORTICITY IS NOW
0261 CALCULATED AND ADDED ON
0262
0263 FAC = FAC+C2*(V(L1)+V(L2)+V(L3)+V(L4)+V(L5)+V(L6)-6.0*V(L))
0264
0265 THE CONTRIBUTION FROM THE CURL OF THE WIND IS ADDED ON
0266
0267 FAC = FAC + T(L)
0268
0269 THE CONTRIBUTION OF THE BOTTOM STRESS IS ADDED ON AND THE
0270 RESULT STORED IN G2(L)
0271
0272 G2(L) = FAC - (C3/H(L)) * (V(L) + ((HC1(L) * (S(L1) - S(L4) + 0.5
0273 * (S(L2) - S(L5) - S(L3) + S(L6)))) + (HC2(L) * (S(L2) - S(L5)
0274 + S(L3) - S(L6))))
0275
0276 1 CONTINUE
0277 2 CONTINUE
0278
0279 THE NEW BOUNDARY VALUES FOR THE VORTICITY ARE
0280 CALCULATED IN THIS SECTION
0281 FIRST THE LOCAL CHANGE OF VORTICITY IS CALCULATED FOR ALL BOUNDARY
0282 POINTS EXCEPT WHERE INFLOW OCCURS, THOSE VALUES DO NOT CHANGE
0283 WITH TIME.
0284
0285 DO 8 I = 1,NB
0286 L = IBC(7,I)
0287 LA(1) = L+1
0288 LA(2) = L-N+1
0289 LA(3) = L-N

```

CCCC

CCCC CCCC CCCCC

910

CCCCCCCC

```

0289 LA(4) = L-1
0290 LA(5) = L+N-1
0291 LA(6) = L+N
0292 FAC = 0.0
0293 TRI = 1.0
0294 DO 84 J = 1,6
0295 K = J+1
0296 IF(K.EQ.7) K = 1
0297 M = J-1
0298 IF(M.EQ.0) M = 6
0299
0300 HERE THE CONTRIBUTION FROM ADVECTION IS CALCULATED IF THE TRIANGLE
0301 IS INTERIOR TO THE MODEL
0302
0303 IF(IBC(J,I).EQ.0.OR.IBC(K,I).EQ.0) GO TO 81
0304 L1 = LA(J)
0305 L2 = LA(K)
0306 FAC = FAC + (S(L2)-S(L1))*((C1*V(L2)+F(L2))/H(L2)) +
0307 (C1*V(L1)+F(L1))/H(L1))/(2.0*AREA)
0308 E
0309
0310 HERE THE CONTRIBUTION FROM DIFFUSION PARALLEL THE BOUNDARY IS
0311 CALCULATED
0312
0313 IF(IBC(J,I).NE.3.AND.IBC(J,I).NE.4) GO TO 811
0314 L1 = LA(J)
0315 FAC = FAC + C2*(V(L1)-V(L))/2.0
0316
0317 HERE THE CONTRIBUTION OF DIFFUSION FROM THE INTERIOR IS
0318 CALCULATED
0319
0320 IF(IBC(J,I).NE.1.AND.IBC(J,I).NE.2) GO TO 812
0321 L1 = LA(J)
0322 FAC = FAC + C2*(V(L1)-V(L))
0323 CONTINUE
0324
0325 HERE THE DIFFUSION NORMAL TO THE BOUNDARY IS CALCULATED IF A NO
0326 SLIP CONDITION IS USED. NOTE LENGTH FACTORS CANCEL OUT, NO EXTRA
0327 COEFFICIENTS ARE NEEDED.
0328
0329 IF(IBC(J,I).NE.2) GO TO 82
0330 IF(IBC(M,I).EQ.2.AND.IBC(K,I).EQ.2) GO TO 82
0331 IF(IBC(M,I).EQ.2) GO TO 813
0332 L1 = LA(J)
0333 L2 = LA(M)
0334 FAC = FAC + C2*(V(L1)-0.5*(V(L2)+V(L)))
0335 IF(IBC(K,I).EQ.2) GO TO 82
0336 L1 = LA(J)
0337 L2 = LA(K)

```



```

C      FAC = FAC + C2*(V(L1)-0.5*(V(L2)+V(L)))
C      NOW THE POSSIBILITY OF VORTICITY BEING ADVECTED OUT OF THE MODEL
C      IS TAKEN CARE OF.
C 82      IF(IBC(J,I).NE.4) GO TO 83
C      L1 = LA(J)
C      FAC = FAC - ABS(S(L1)-S(L))*((C1*V(L1)+F(L1))/H(L1))+(C1*V(L)
1      +F(L))/H(L))*0.5/AREA
C      HERE THE NUMBER OF OUTSIDE POINTS ARE COUNTED FOR THE AREA
C      CORRECTION
C 83      IF(IBC(J,I).EQ.0) TRI = TRI + 1.0
C 84      CONTINUE
C      NOW THE LOCAL CHANGE IS CORRECTED FOR AREA
C      G2(L) = FAC*6.0/(6.0-TRI)
C      CONTINUE
C 8      THE NEW BOUNDARY VALUE FOR THE VORTICITY IS CALCULATED
C      USING THE ADAMS-BASHFORTH SCHEME AND G2 IS TRANSFERRED
C      TO G1
C 80      DO 80 I = 1,NB
C      L = IBC(7,I)
C      V(L) = V(L) + DT*(1.5*G2(L)-0.5*G1(L))
C      TRI = 1.0
C 888      DO 888 J = 1,6
C      IF(IBC(J,I).EQ.0) TRI = TRI + 1.0
C      CONTINUE
C      VORT = VORT + V(L)*(6.0-TRI)/H(L)
C      G1(L) = G2(L)
C      THE NEW VALUE OF THE VORTICITY IS CALCULATED AT ALL
C      INTERIOR POINTS USING THE ADAMS-BASHFORTH METHOD AND
C      THE PRESENT VALUE OF THE LOCAL CHANGE IS TRANSFERRED
C      FROM G2 TO G1 TO BE USED IN THE NEXT TIME STEP
C 12      DO 12 K = 1,M2
C      I = IA(K)
C      J = JA(K)
C 11      DO 11 L = I,J
C      V(L) = V(L)+DT*(1.5*G2(L)-0.5*G1(L))
C      VORT = VORT + V(L)*6.0/H(L)
C      G1(L) = G2(L)
C      CONTINUE
C 11
C 12

```


0385
0386
0387
0388
0389
0390
0391
0392
0393
0394
0395
0396
0397
0398
0399
0400
0401
0402
0403
0404
0405
0406
0407
0408
0409
0410
0411
0412
0413
0414
0415
0416
0417
0418
0419
0420
0421
0422
0423
0424
0425
0426
0427
0428
0429
0430

THE NEW VALUE OF THE STREAM FUNCTION IS OBTAINED
VIA THE RELAXATION OF THE NEW VORTICITY FIELD. A
SWEEP PROCEDURE IS STARTED AND 100 SWEEPS IS SET AS
THE UPPER LIMIT ON PASSES THROUGH THE GRID

```
ITER = 100
DO 15 II = 1,100
ERR = 0.0
DO 14 K = 1,M2
I = IA(K)
J = JA(K)
DO 13 L = I,J
L1 = L+1
L2 = L-N+1
L3 = L-N
L4 = L-1
L5 = L+N-1
L6 = L+N
HO = H(L)
FAC = 1.33333*(S(L1)/(H(L1)+HO)+S(L2)/(H(L2)+HO)
E   +S(L3)/(H(L3)+HO)+S(L4)/(H(L4)+HO)+S(L5)/(H(L5)+HO)
E   +S(L6)/(H(L6)+HO)-S(L)*RES(L))-V(L)
FAC = FAC/(1.33333*RES(L))
S(L) = S(L)+R*FAC
FAC = ABS(FAC)
IF(FAC.GT.ERR) ERR = FAC
CONTINUE
CONTINUE
```

THE CONVERGENCE IS NOW CHECKED AND IF THE MAX
RESIDUE IS LESS THEN CON THE ITERATION LOOP IS EXITED

```
IF(ERR.GT.CON) GO TO 15
```

```
ITER = II
GO TO 155
```

```
CONTINUE
```

```
GO TO 6
```

```
CONTINUE
IF(IPUNCH.EQ.0) GO TO 17
```

```
WRITE(7,115) S
```

```
WRITE(7,115) V
```

```
WRITE(7,115) G1
```

```
CONTINUE
```

```
STOP
```

```
END
```

13
14

C
C
C
C

15
155
16

17

```

C C C C C
SUBROUTINE GRAOUT(LV,LO,NOUT,A,NM,IA,JA,M2,N,BLANK)
DIMENSION LV(20),LO(NOUT),A(NM),IA(M2),JA(M2)
THIS SUBROUTINE TAKES THE INTERIOR VALUES IN ARRAY A SCALES
THEM, TRANSFORMS THEM TO AN ALPHA CODE AND PRINTS
THEM OUT IN A CARTESIAN GRID
M = NM/N
DO 1 K = 1,NOUT
LO(K) = BLANK
K = IA(1)
AMAX = A(K)
AMIN = AMAX
DO 3 K = 1,M2
I = IA(K)
J = JA(K)
DO 2 L = I,J
IF(A(L).GT.AMAX) AMAX = A(L)
IF(A(L).LT.AMIN) AMIN = A(L)
CONTINUE
ADIF = AMAX-AMIN
IF(ADIF.EQ.0.0) GO TO 8
DO 5 K = 1,M2
I = IA(K)
J = JA(K)
DO 4 L = I,J
LL = 2*L-1+((L-1)/N)*(M-1)
NN = IFIX(19.999*(AMAX-A(L))/ADIF)
LO(LL) = LV(NN+1)
CONTINUE
WRITE(6,6) LO
THIS FORMAT CARD MUST BE CHANGED FOR DIFFERENT NM VALUES
THE COEFFICIENT BEFORE THE A2 SHOULD BE (2N-1) + (M-1)
FORMAT(1H0,19A2)
RETURN
WRITE(6,9)
FORMAT(47H THE ARRAY HAD A CONSTANT VALUE NO GRAPH GIVEN )
RETURN
END
C C C C C
1
2
3
4
5
6
7
8
9
0431
0432
0433
0434
0435
0436
0437
0438
0439
0440
0441
0442
0443
0444
0445
0446
0447
0448
0449
0450
0451
0452
0453
0454
0455
0456
0457
0458
0459
0460
0461
0462
0463
0464
0465
0466
0467
0468
0469
0470
0471
0472

```

DISTRIBUTION

	No. of Copies
Chief of Naval Research, Code 415 Office of Naval Research Arlington, Virginia 22217	3
Defense Documentation Center Cameron Station Alexandria, Virginia 22314	12
Library Naval Postgraduate School Monterey, California 93940	2
Dean of Research Administration Naval Postgraduate School Monterey, California 93940	2
Director, Naval Research Laboratory Attn: Technical Information Officer Washington, D. C. 20390	6
Chief of Naval Research, Code 480 Office of Naval Research Arlington, Virginia 22217	1
Department of the Army Washington, D. C. 20315	1
Cold Regions Research & Engineering Laboratory Post Office Box 282 Hanover, New Hampshire 03755	1
Dr. Reid A. Bryson Department of Meteorology University of Wisconsin Madison, Wisconsin 53706	1
Air University Library AUL3T-63-735 Maxwell Air Force Base Alabama 36112	1

	No. of Copies
Naval Academy Library Annapolis, Maryland 21402	1
Director Naval Arctic Research Laboratory Barrow, Alaska 99723	1
Dr. Waldo Lyon Arctic Submarine Laboratory Naval Undersea R & D Center San Diego, California 92132	1
Professor Norbert Untersteiner Dept. of Atmospheric Sciences University of Washington Seattle, Washington 98105	1
Executive Director Brig. H. W. Love The Arctic Institute of North America 3458 Redpath Street Montreal 109, Quebec, Canada	1
Director, Institute of Polar Studies Ohio State University 125 South Oval Drive Columbus, Ohio 43210	1
Miss Maret Martna, Director Arctic Bibliography Project 406 East Capitol Street, N. E. Washington, D. C. 20003	1
Dr. Kenneth L. Hunkins Lamont-Doherty Geological Observatory Torrey Cliffe Palisades, New York 10964	1
Chief of Naval Research Office of Naval Research, Code 466 Arlington, Virginia 22217	1
Chief of Naval Research Office of Naval Research, Code 468 Arlington, Virginia 22217	1

No. of Copies

Mr. Beaumont Buck
Delco Electronics
General Motors Corp.
6767 Hollister Avenue
Goleta, California 93107

1

Dr. Kou Kusunoki
Polar Division
National Science Museum
Ueno Park
Tokyo, Japan

1

Dr. Louis O. Quam
USARP Chief Scientist
National Science Foundation
Washington, D. C. 20550

1

Miss Moira Dunbar
Defence Research Board/DRFO
125 Elgin Street
Ottawa 4, Ontario, Canada

1

Dr. A. R. Milne
Pacific Naval Laboratory
Defence Research Board
Department of National Defence
Esquimalt, British Columbia, Canada

1

Dr. Hector R. Fernandez
Department of Biology
University of Southern California
Los Angeles, California 90007

1

Dr. Norman J. Wilimovsky
Institute of Fisheries
Univ. of British Columbia
Vancouver 8, British Columbia
Canada

1

Mr. Louis Degoes
Executive Secretary
Committee on Polar Research
National Academy of Sciences
2101 Constitution Avenue, N. W.
Washington, D. C. 20418

1

	No. of Copies
Chief of Naval Operations DP-07T Department of the Navy The Pentagon Washington, D. C. 20350	1
Dr. V. J. Linnenbom Naval Research Laboratory Code 7500, Bldg. 58, Room 246 Washington, D. C. 20390	1
Mr. J. D. Fletcher Office of Polar Programs 1800 G. Street, N. W. Washington, D. C. 20550	1
Director Woods Hole Oceanographic Institution Woods Hole, Massachusetts 01823	1
Northern Affairs Library Kent-Albert Building Ottawa, Ontario, Canada	
Dr. Donald W. Hood Institute for Marine Science University of Alaska College, Alaska 99735	1
Dr. Lawrence Coachman Department of Oceanography University of Washington Seattle, Washington 98105	1
Dr. T. Saunders English Department of Oceanography University of Washington Seattle, Washington 98105	1
Dr. Max J. Dunbar Marine Sciences Centre McGill University Montreal 110, Quebec, Canada	1

	No. of Copies
Dr. David Clark Department of Geology University of Wisconsin Madison, Wisconsin 53706	1
Office of the Oceanographer Programs Division Code N-6 732 N. Washington Street Alexandria, Virginia 22314	1
Dr. Gunnar Thorson Marine Biological Laboratory University of Copenhagen Gronnehave, Helsingor, Denmark	
Librarian Defence Research Board of Canada Ottawa, Ontario, Canada	1
Director Arktisk Institut Kraemerhus L. E. Bruunsvej 10 Charlottenlund, Denmark	1
Director Norsk Polar Institute Observatoreigt. 1 Oslo, Norway	1
Librarian Scott Polar Research Institute Cambridge, England	1
Naval Ships System Command Attn: Code 205 Department of the Navy Washington, D. C. 20360	1
Librarian Technical Library Navy Underwater Sound Laboratory Fort Trumbull, New London, Conn 06320	1

	No. of Copies
Librarian (Code 1640) U. S. Naval Oceanographic Office Suitland, Md. 20390	1
Librarian U. S. Naval Electronics Laboratory Center San Diego, California 92152	1
Librarian, Technical Library U. S. Naval Undersea Warfare Center 3202 E. Foothill Blvd. Pasadena, California 91107	1
Librarian, Technical Library Division Naval Civil Engineering Laboratory Port Hueneme, California 93041	1
Dr. Johannes Wiljhelm Det Danske Meteorologisk Institut Gamlehave Alle 22 Charlottenlund, Denmark	1
Library National Museums of Canada McLeod and Metcalfe Streets Ottawa 4, Ontario, Canada	1
Dr. C. J. Wang, Director Advanced Engineering Office Advanced Research Projects Agency Arlington, Virginia 22217	1
Director, U. S. Naval Research Laboratory Attn: Library, Code 2029 (ONRL) Washington, D. C. 20390	6
Dr. Knut Aagaard Department of Oceanography University of Washington Seattle, Washington 99105	1
J. B. Matthews Institute of Marine Sciences University of Alaska College, Alaska 99701	1

No. of Copies

Chief Scientist 1
 ONR Branch Office Chicago
 536 South Clark Street
 Chicago, Illinois 60605

Chief Scientist 1
 ONR Branch Office Boston
 495 Summer Street
 Boston, Mass. 02210

Chief Scientist 1
 ONR Branch Office, Pasadena
 1030 East Green Street
 Pasadena, California 91101

Director 3
 Advanced Research Projects Agency
 Attn: Program Management
 Washington, D. C. 20301

Mr. Ralph Cooper, Code 438 1
 Office of Naval Research
 Arlington, Virginia 22217

John R. Guala 1
 Dept. of Mechanical and Aerospace Engineering
 University of Delaware
 Newark, Delaware 19711

Don L. Boyer 1
 Atmospheric Sciences Section
 National Science Foundation
 1800 G Street
 Washington, D. C.

A. Brandstetter, Senior Research 1
 Water and Land Resources Dept.
 Battelle Memorial Institute
 Pacific Northwest Laboratories
 P. O. Box 999
 Richland, Washington 99352

	No. of Copies
M. Moens Universite de Louvain Institut D'Astronomie et de Geophysique Centre de Physique Nucleaire Parc D'Arenberg - Avenue Cardinal Mercier 3030 Haverle-Louvain Belgique	1
J. B. Matthews Institute of Marine Science University of Alaska College, Alaska 99701	2
Mr. Robert Peloquin U.S.N.O.C. Office Code 7300 Washington, D. C. 20390	
M. A. Selim Union Research Center P. O. Box 76, Brea, California 92621	1
Albert J. Semtner Geophysical Fluid Dynamics Laboratory Princeton University P. O. Box 308 Princeton, N. J. 08540	
Charles D. D. Howard Unies Ltd. 565 Roseberry Street Winnipeg, Canada R3HOT3	1
Dr. Drew Rothrock AIDJEX Office Div. of Marine Resources University of Washington Seattle, Wash. 98105	1
Chairman Department of Oceanography Naval Postgraduate School Monterey, California	1

No. of Copies

Professor J. A. Galt
Department of Oceanography
Monterey, California 93940

6

DOCUMENT CONTROL DATA - R & D

(Security classification of title, body of abstract and indexing annotation must be entered when the overall report is classified)

1. ORIGINATING ACTIVITY (Corporate author)

Naval Postgraduate School
Monterey, California 93940

2a. REPORT SECURITY CLASSIFICATION

Unclassified

2b. GROUP

3. REPORT TITLE

The Development of a Homogeneous Numerical Ocean Model for the Arctic Ocean

4. DESCRIPTIVE NOTES (Type of report and, inclusive dates)

5. AUTHOR(S) (First name, middle initial, last name)

J. A. Galt

6. REPORT DATE

July 1972

7a. TOTAL NO. OF PAGES

59

7b. NO. OF REFS

21

8a. CONTRACT OR GRANT NO.

b. PROJECT NO.

c.

d.

9a. ORIGINATOR'S REPORT NUMBER(S)

NPS-58G172071A

9b. OTHER REPORT NO(S) (Any other numbers that may be assigned this report)

10. DISTRIBUTION STATEMENT

This document has been approved for public release and sale; its distribution is unlimited.

11. SUPPLEMENTARY NOTES

12. SPONSORING MILITARY ACTIVITY

Naval Postgraduate School
Monterey, California 93940

13. ABSTRACT

A numerical ocean model driven by surface stress and a source-sink distribution is developed for a homogeneous ocean. Non-linearities, lateral friction and bottom friction are included. The basin shape can be varied to accommodate a large variety of configurations. Variable bathymetry and sources/sinks around the perimeter are included. The numerical scheme is conditionally stable and has second order accuracy in space and time.

A number of test cases are run to explore the dynamic significances of the various processes represented. The possible influence of these processes on the circulation of the Arctic ocean are discussed.

14

KEY WORDS

LINK A

LINK B

LINK C

ROLE

WT

ROLE

WT

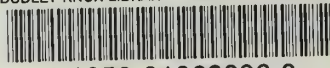
ROLE

WT

Ocean Circulation
Numerical Modeling
Arctic Ocean

U146264

DUDLEY KNOX LIBRARY - RESEARCH REPORTS



5 6853 01068096 0